Nano-curcumin Capped Au/ZnO Nanocomposite: A Promising Approach to Protect from Staphylococcus Aureus Infection through Inhibits Production of α-Hemolysin

Majid Jabir (100131@uotechnology.edu.iq)
University of Technology, Bagdad, IRAQ https://orcid.org/0000-0003-0759-8298
Majid Jabir
University of Technology, Bagdad, IRAQ
Taha M. Rashid
University of Technology, Bagdad, IRAQ
Uday M. Nayef
University of Technology, Bagdad, IRAQ
Duha A. Kadhim
Mustansiriyah University Bagdad

Research Article

Keywords: Curcumin, Au@ZnO nanocomposite, Laser ablation in liquid, Antibecterial activity, S.aureus, α-Hemolysin

Posted Date: May 13th, 2021

DOI: https://doi.org/10.21203/rs.3.rs-516417/v1

Abstract

Gold with Zinc Oxide nanoparticles (Au@ZnO NPs) were prepared by laser ablation then capped with Curcumin nanoparticles. The ability of Nano-curcumin-Au/ZnO nanocomposite as a promising antibacterial agent was tested against *Staphylococcus aureus*. Cur-Au@ZnO NPs were characterized by TEM, FTIR spectroscopy, and Uv-spectroum. TEM image of Au@ZnO NPs has grain size almost 27–38 nm and it increased after capped Nano-curcumin to 72–113 nm. Agar well diffusion method was used to evaluate the antibacterial activity of Cur-Au@ZnO against *S.aureus*. The activity of Cur-Au@ZnO NPs was determined via detection of (ROS) using (AO/EtBr) staining assay. The bacterial cytoplasmic membrane and nucleic acid were penetrated by tested nanoparticles, resulting in bacterial strain destruction. The results showed that Cur-Au@ZnO NPs as a novel DNA-mediated antibacterial agent. The Cur-Au@ZnO were observed to destroy the bacterial cells by permeating the bacterial nucleic acid and cytoplasmic membrane, resulting in the loss of cell-wall integrity, nucleic acid damage, and increased cell-wall permeability. Furthermore, in the present study we investigated the activity of Cur-Au@ZnO NPs against bacterial α-Hemolysin toxin. Western blot were used to measure the effect of Cur-Au@ZnO NPs on α-Hemolysin produced by *S. aureus*. The effectiveness of Cur-Au@ZnO NPs against human alveolar epithelial cell injury by α-Hemolysin was tested using live ⁄ dead staining. Also, we demonstrated the role of Cur-Au@ZnO NPs against *S. aureus* through histopathology examination in a mouse model. Taken together, Cur-Au@ZnO NPs is a potent inhibitor of α-hemolysin secreted by *S. aureus*. So, Cur-Au@ZnO NPs mediated inhibition of α-Hemolysin production may offer a new strategy in combating pathogen infections. The Cur-Au@ZnO could serve as a potential antibacterial agent in future for biomedical and pharmaceutical applications.

1. Introduction

Nanoparticles may be used as structural components or composites, and they have a much wider range of functions than bulk materials. The following parameters define the physical and chemical properties of metallic nanoparticles: size, shape, and composition [1–2]. Recent attention has been given to the efforts to nanoparticle colloids, in which case of cell delivery, the functionality and various fields of study in drug synthesis, diagnostics, and research, among others, for their specific properties have been synthesized. In contrast to conventional wet chemical synthesis, pulsed laser ablation (PLA) may produce single-step pure colloids for a wide range of materials, without any chemical precursors or preservatives. Often, semiconductors have been demonstrated in a number of liquids [3–4]. To enhance the controllability of methods of forming nanostructured materials, the composition of the surrounding medium and the laser parameters can be used to monitor the structure and size of the nanostructure [5]. The technique is based on intense nanosecond pulsed lasers in a focused state for creating a particle with a distinct property in the nanoscale[6]. Metal nanoparticles (NPs) have been extensively investigated for decades due to their specific features and their potential usage in catalysis, electronics, information storage, and biomedical applications [7–8]. Gold nanoparticles (Au NPs) are a more promising material that has attracted interest due to their obvious benefits. To begin, we can easily synthesize Au NPs in a

variety of shapes ranging from 1 nm to more than 100 nm in diameter, including spherical, rod-like, cage-like, and so on. Au nanoparticle's optical and electrical properties are highly dependent on their shape and scale[9], Second, since Au NPs have a negative charge, they can be easily functionalized with a wide variety of biomolecules, including drugs, genomes, and targeting ligands [10]. Thirdly, Au NPs are nontoxic and biocompatible [11]. Fourthly, Au NPs exhibit a unique surface effect, are extremely small in size, exhibit macroscopic quantum tunneling, and contain surface plasmon resonance (SPR) bands [12]. All of these properties have made Au NPs the most promising material for a variety of biomedical applications, including biosensing, molecular imaging, and drug delivery. Detailed information on the preparation and use of Au NPs in biosensing has been published elsewhere [13]. Zinc Oxide Nanoparticles are commonly employed in a wide range of sectors due to their particular chemical and physical properties as one of the most significant metal oxide nanoparticles [14–15]. Moreover, ZnO NPs have superior UV-blocking, antibacterial and antimicrobial properties. The finished fabrics thus showed the attractive functions of ultraviolet and visible light resistance, antibacterial agent and deodorant in the textile industry. Surfaces are becoming very common and can be used in various applications to prevent degrading factors including soil, teats or other pollutants from protecting the material's surface texture, window glasses and other open-air products. Hydrophilic or hydrophobic conduct can remove deposited impurities [16]. Curcumin (1, 7-bis (4-hydroxy-3-methoxyphenyl)-1, 6-heptadiene-3, 5-dione) obtained from curcuma longa rhizomes possesses a variety of biological and pharmacological properties [17]. It exhibits a heavy proclivity for chelating with metal ions. Due to its incompatibility with water (20 g/mL), it has a low bioavailability and absorption in biological applications [18]. To increase curcumin's bioavailability, numerous delivery modes have been established, including nanoparticles, liposomes, microemulsions, vesicles, complexation with phospholipids, and inclusion complexes based on cyclodextrin[19]. *S. aureus*, a gram-positive bacterial strain. It is one of the one of the notable serious medical pathogens. *S.aureus* responsible for a variety of life-threatening infections, such as endocarditis, osteomyelitis, keratitis, sepsis syndrome and pneumonia [20]. In addition, *S.aureus* one of the leading aetiological agents of ventilator-associated pneumonia, *S. aureus* is partially responsible for the intensive care environment and is increasingly recognized as an important cause of community-acquired pneumonia, affecting a population of otherwise healthy adults and children [21–22]. The development of therapeutic options is imperative while we await new antimicrobial agents or new therapeutic approaches for the prevention and treatment of *S. aureus*. The pathogenicity of *S. aureus* is partially attributed to the expression of a considerable repertoire of virulence factors, including catalase, fibrinolysin, superoxide dismutase, hyaluronidase, Hemolysin (alpha, beta, delta and gamma), epidermolytic toxins and superantigens [23]. α-Hemolysin (encoded by the hla gene), which is secreted from most pathogenic strains of *S. aureus* as a 33.2-kDa water-soluble monomer, attacks virtually all mammalian cells through the formation of stable, amphiphilic transmembrane pores [24–25]. This poreforming toxin is thought to be an important protein that mediates tissue damages of *S. aureus* [26], have demonstrated that α-hemolysin damages the air–blood barrier of the lung in a rat model of *S. aureus* induced pneumonia [27], have reported that *S. aureus* mutant strains lacking α-Hemolysin are defective in inducing pneumonia-related mortality. α-Hemolysin has been shown to be a pivotal mediator in ocular infections caused by *S. aureus* via a multitude mechanism [28]. On the basis of these considerations, targeting α-hemolysin may

be a potential alternative strategy against *S. aureus* pneumonia. The nanomedicines have been an emerging therapeutic approach to conquer the obstacles of treatment of *S. aureus* infections with their ability of inhibition of the formation of biofilm [29], penetration of cell and biofilm membrane, enhanced intracellular retention [30] and improved antibacterial activity of the loaded antimicrobial agents. Nanoparticles can passively accumulate in certain organs and infection site because of their special characteristics, such as nanosize, surface charge, and large specific surface area. The modified nanoparticles could further enhance the transmembrane performance of their payload drug by actively realizing the receptors of host cells and bacterial cells. Currently, many antimicrobial agents are incorporated into or conjugated with nanocarriers to enhance the pharmacologic activities against sensitive and resistant *S. aureus* to reduce the side effects of the drug [31–33]. Therefore, nanoparticle drug delivery systems proved an ideal weapon to overcome the challenges of *S. aureus* infection that we faced. This study designed to study the effect of Cur-Au@ZnO CSNPs against *S.aureus*. The results showed that the Cur-Au@ZnO NPs is a promising agent against *S. aureus* through inhibits of α-Hemolysin. So, Cur-Au@ZnO NPs may offer a new strategy in combating pathogen infections.

2. Materials And Methods

2.1. Chemicals and materials

Cold (Au) a high purity was purchased as a pellet from the local market in Baghdad, Iraq. Zn purchased as a powder and It was pressed with a 10 bar hydraulic press to get a pellet. Fresh Curcumin (1,7-bis-(4-hydroxy-3-methoxyphenyl)-1,6 heptadiene-2,5-dione), Curcuma longa plants is a bright yellow chemical. It's the main curcuminoid in turmeric (Curcuma longa), which belongs to the Zingiberaceae ginger band. It's available as a herbal supplement, a beauty product, a food flavoring, and a food coloring, was purchased from the local market in Baghdad, Iraq.

2.2 Preparation of Au/ZnO core/shell nanoparticles

The Au NPs was made from a high purity metal plate, fixed to the base of the glass cell, and added 3 ml of deionized water (DW). Nd:YAG (1064nm, 9ns, 200 pulse, 1Hz) radiated energy is centered on the surface of the target. PLA in liquid has been performed at room temperatures to obtain a colloidal solution of gold nanoparticles, Zn has been used as a pellet fixed in a glass cell containing a colloidal Au NP solution irradiation with the same condition of Au NPs. The post-laser 532 nm with 300 pluses was used after preparing Au/ZnO as a core/shell nanoparticle.

Figure 1 shows a soft particle produced when the beam is concentrated on targets using a 100mm convex lens. The dispersion in water takes on a variety of colors, depending on the laser energy.

2.3. Preparation of Curcumin-Au/ZnO NPs

The synthesized of prepared curcumin from mixing 5 gm of curcumin with 50 ml of distilled water (DW) by chemical method using the ultrasonic device at 200 Hz, 50^{o}C and cooling to room temperature. Then, it observes the change of dark yellow to light yellow this represented to formation nanocurcumin. After

that, the solution result was centrifuged at 4000 rpm for 10 minutes. The solution results were stored in sealed tubes.

2.4. Characterization of Curcumin loaded Au/ZnO

The absorption spectra of the Au and ZnO NPs solution were investigated using a spectrophotometer (Model-Shimadzu, 1200) with a double UV-vis beam at different conditions in the spectral range (200–1100) nm. The solutions are placed in a quartz cell (optical path equal 1cm). The optical properties of ZnO and Au NPs colloids were discovered. The size and shape of NPs were observed using a transmitted electron microscope (TEM by DayPeronic company, Tehran/Iran).

2.5. Antibacterial activity of Cur-Au/ZnO NPs

The antibacterial activity of the prepared

Cur- Au/ZnO NPs was tested using an agar well diffusion technique against human pathogen *S. aureus*. 20 mL of Muller-Hinton (M-H) was used poured into petri dishes before the culturing process began. A sterile wire loop was used to capture the bacteria from their stock cultures. Following the culturing of the bacterial strains, a sterile tip was used to bore six mm-diameter wells in the agar plates.The tested nanoparticles were added into the bored plates. After culturing, the plates were incubated at 37° C over night. The tests were done in triplicate. To assess how Cur- Au/ZnO NPs affects the growing curve of bacteria, they were cultured on the M-H agar plates at 37° C, the collection freshly cultured plates inoculations composed of 50 mL of nutrient broth. The bacterial grew until the nutrient broth reached optical density (OD) of 0.1 at 600 nm, which is equivalent to bacterial concentration of corresponds a bacterial concentration of 10^8 (CFU/mL). Then, bacterial cultures (1mL) were added to the nutrient broth and was supplemented with Cur- Au/ZnO NPs and incubated at 37° C for 12 h with slight agitation. A spectrophotometer was used to determine bacterial growth by measuring the OD [34–36].

2.6. Morphology of Bacterial Strain Using SEM

The changes in the morphology of the *S.aureus* were observed using a scanning microscope. Both NPs treated and untreated bacteria strains were centrifuged at 500 rpm and then washed 3 times using PBS (pH 7.3). A thin suspension film was made on a clean silicon wafer slide. They were then air-dried at ambient temperature and then they were fixed using 1 mL of a fixing buffer. Once they were fixed, the slides were incubated at 37º C for 1.30 hours, and the water was removed using methanol (ascending grade), dried in open air, and then fixed on the SEM stubs, and they were coated with gold for 5 minutes, about 20 nm of gold was left on the cells surface. SEM (TESCAN, Vega III, Czech Republic) was used to examine the gold-coated cells [37].

2.7. Detection of reactive oxygen species (ROS)

The ROS released by treated nanoparticles bacterial cells was observed using an acridine orange/ethidium bromide (AO/EB) staining technique. A fluorescent microscope was used to measure the antibacterial activity of the Cur- Au/ZnO NPs against tested bacterial strain. To distinguish bacterial cell

viability after treatments a AO/EtBr staining procedure was done. 50 µL bacterial suspension of both treated and untreated was mixed with 50 µL (prepared from 10 µg/mL AO/EtBr stock solution) and was left for about 2 minutes. Staining procedure followed, after which a thin film of the mixture was applied on a glass slide and then observed under an immunofluorescent microscope. For the living cells, the Acridine Orange-stained fluoresce green while for the dead cells the Ethidium Bromide-stained fluorescence red [38].

2.8. Bacterial adherence assay

The cells of the rat embryonic fibroblast (REF) were cultured in twelve well tissue culture plates at density $1*10^5$. These cells were infected with bacteria strains at MOI ratio 200:1 in the absence and presence of the Au, ZnO, Au/ZnO NPs, and Cur-Au/ZnO NPs. The plates were then incubated for 2 hour in 5% CO_2 incubator at 37° C. After incubation, they were washed thrice with PBS. PFA was used to fix the cells for 15 minutes, and later crystal violet stain was used to stain the cells for 15 min.

2.9. Bacterial invasion assay

A 12 well tissue was also used to grow Rat embryonic fibroblast (REF) cells, which were later infected with bacterial strains in absence and presence of the Au, ZnO, Au/ZnO NPs, and Cur-Au/ZnO NPs for 2 hours. The REF cells left after culture media was removed were washed thrice with PBS. A fresh RPMI-1640 medium consisting of gentamicin 100 µg/ml was added and the mixture incubated for 2 hours. The cells were then washed thrice with PBS, broken down by for 20 minutes using 0.1% Triton X-100 at 37° C. For each well, 10 µl was drawn and added to the nutrient agar for bacteria colonies to grow, which were counted after 20 h. The bacteria invasion efficiency was determined as the mean number of bacterial in each well. This bacterial invasion essay was conducted in triplicate.

2.10. Immunoblot analysis for a-Hemolysin

Samples were separated on 12% SDS–PAGE after boiling in loading-reducing buffer and transferred to polyvinylidene fluoride membranes. Then, the membrane was blocked by incubated overnight at 4_C in 5% bovine serum albumin in PBS to block free protein- binding sites, and then samples were incubated with rabbit polyclonal antibody to a-Hemolysin (diluted 1 : 1000). The samples were washed 3 times with PBs. Then, bound antibody was detected with horseradish peroxidase-conjugated anti-rabbit antiserum at concentration 1:2000. The blots were developed using Amersham ECL Western blotting detection reagents.

2.11. Live / dead and cytotoxicity assays

A549 human lung epithelial cells plated in RPMI-1640 medium supplemented with 10% foetal bovine serum at a density of 1×10^1 cells per well in 96-well plates. A549 cells were co-cultured with 100 µl of *S.aureus* suspension in the presence and absence of the Au, ZnO, Au/ZnO NPs, and Cur-Au/ZnO NPs. After 8 h of incubation at 37^0C, cells were either stained with live ⁄ dead (green ⁄ red) reagent.

Microscopic images of stained cells were captured using a confocal microscope. Cell viability was determined by measuring lactate dehydrogenase (LDH) release using Cytotoxicity Detection Kit (LDH) according to the manufacturer's directions. LDH activity was measured on a microplate reader.

2.12. Lung infection model

Mice were handled according to the experimental practices and standards approved by the Animal Research Ethics Committee at university of technology. For lung infection, 8–10 week-old male mice were anaesthetized. Then, *S. aureus* suspension was dropped into the left nare. Mice infected with *S. aureus* were subcutaneously administered with Au, ZnO, Au/ZnO NPs, and Cur-Au/ZnO NPs 2 h after infection and then at 12-h intervals thereafter for a total of 4 doses. The control mice received 100 µl sterile PBS on the same schedule. Then, mice were euthanized with anesthesia followed by cervical dislocation before lungs were placed in 1% formalin. Formalin fixed tissues were processed, stained with hematoxylin and eosin, and visualized by light microscopy [39].

2.13. Statistical analysis

The unpaired t-test was used to analyze our results as allows comparison of experimental groups at a significant p-value of < 0.05[40].

3. Result And Dissection

3.1. Characterization of Nanoparticles

Figure (2) Show TEM images of prepared nanoparticles, the image show that Au as a dark semi spherical with average size 18nm as in Fig. 2- A, While Fig. 2-B, refer to ZnO NPs, shiny dark as a cross-linked refer to pure ZnO NPs as adherence on Au NPs with average size 25nm, as in Fig. 2-C. D, refer to the curcumin as irregular spherical size as a nanocluster, while, E) shows pure curcumin when mixing with Au/ZnO NPs, appearances the important role of curcumin played a capping of Au/ZnO NPs. The FTIR spectra were recorded in the 400–4000 cm-1 spectral range. Figure 3 shows the FTIR spectra of Au/ZnO nanocomposites. Several bands can be found in the FTIR spectra of the samples [41, 42]. The large and wide band between 3200 and 3600 cm-1 is assigned to the characteristic stretching vibration mode of the water O–H, which changes as the concentration of Au nanoparticles increases. The presence of CO2 molecules in the ambient air causes bands around 2076 cm-1. Carbon dioxide O = C = O stretching is represented by the small peak at 2356 cm-1 and 2333 cm^{-1}. The O–H bending vibration mode is assigned to the strong band near 1640 cm-1 for Au, ZnO, and Au/ZnO. The spectrum of pure curcumin and Cur-Au/ZnO CSNPs is shown in Fig. 5B, with the orange line referring to active groups for pure curcumin. The band seen at 1640 cm-1 is caused by the uncoordinated phen's ring vibrations. The peaks at 1137 and 3346 cm-1 are possibly due to O–H deformation and stretching due to moisture adsorbed on the NP surface, respectively [43]. When Cur-Au/ZnO CSNPs are mixed with Au/ZnO NPs, several peaks

disappear, leaving only four main peaks: the broad peak at 670 cm-1 showed the predicted Zn–O stretching vibrations, and the broad peak at 3455 cm-1 is the characteristic O–H stretch [44]. In Fig. 4, the absorbance spectra of the Au, ZnO, Au/ZnO, and Cur-Au/ZnO CSNPs, suspensions are shown. Because of interband transitions and SPR oscillations in Au nanoparticles, the UV–visible absorption spectra of gold nanoparticles display absorptions in the ultraviolet and visible regions, respectively. Au nanoparticles have a plasmon peak at 527 nm. Figures (3) shows the UV absorption peak of ZnO nanoparticles exciton absorption at 330 nm. This finding is identical to previous PLA-prepared ZnO nanoparticles [45]. UV absorption is observed in the Au/ZnO nanocomposites. Due to the low concentration of Au nanoparticles in colloidal solution of ZnO NPs, the strongly damped absorption becomes weak and wide. For Au/ZnO suspension, a large peak with a red shift of 540 nm was observed, which corresponds to the localized SPR of the partially shaped gold nanoparticles. Figure 3-B, show the UV-Visible Spectrophotometer for Pure Cur. and Cur-Au/ZnO CSNPs and show the peak of pure curcumin at 364nm [46] and Cur-Au/ZnO CSNPs appear a broad peak for mixture of nanoparticles and this refer to the pure curcumin play a role as a shell to cover on intensity of absorption for Au and ZnO nanoparticles.

3.2. Antibacterial activity of Cur-Au/ZnO NPs

The antibacterial of Au NPs, ZnO NPs, Cur NPs, Au/ZnO NPs, and Cur-Au/ZnO CSNPs was investigated using *S.aureus.* The inhibition zones after exposing the organisms to tested nanoparticles used were measured and illustrate in Fig. 4. From the result Cur-Au/ZnO NPs found to be effective than ZnO NPs, Au NPs, Cur NPs, and Au/ZnO NPs. Cur-Au/ZnO CSNPs produced an inhibition zone diameter of more than 30 mm against *S.aureus*. The results showed the effect of prepared nanoparticles on the growth of *S.aureus*, especially after 12h of treatment as shown in Fig. 5. The inhibitory effect of Cur-Au/ZnO CSNPs was observed to be more than that of ZnO NPs, Au NPs, Cur NPs as proven by the statistical analysis.

3.3. Bacterial morphology

The effect of Au NPs, ZnO NPs, Cur NPs, Au/ZnO NPs, and Cur-Au/ZnO CSNPs on the structure of *S. aureus* under treatment was assessed using a SEM technique. The images demonstrated that there were differences in the bacteria cell morphology between treated bacterial strains and the untreated samples (control). Untreated control bacterial strain confirmed the cluster-form colonies as in Fig. 7-A. Since *S. aureus* is Gram-positive bacteria and thus exists in clusters, SEM images demonstrated that they were destroyed after they were treated with Au NPs, ZnO NPs, Cur NPs, Au/ZnO NPs, and Cur-Au/ZnO CSNPs as shown in Fig. 7- B, C, D, E, and F. The Au NPs, ZnO NPs, Cur NPs, Au/ZnO NPs, and Cur-Au/ZnO CSNPs was observed to have huge activities on bacterial strains as demonstrated in the bacterial cell structural changes as in Fig. 7. The Au NPs, ZnO NPs, Cur NPs, Au/ZnO NPs, and Cur-Au/ZnO CSNPs had effect on tested microorganisms' outer membrane, as it was observed that the bacterial strain cell membrane had more pores and damage. The damage occurred as a result of osmotic imbalance leading to a leak of bacterial cells and it resulted to changes in morphology, osmotic balance, and cells' structural integrity after it was treated with Au NPs, ZnO NPs, Cur NPs, Au/ZnO NPs, and Cur-Au/ZnO CSNPs. It was observed that in the bacterial strains treated with Au NPs, ZnO NPs, Cur NPs, Au/ZnO NPs, and Cur-Au/ZnO CSNPs there was aggregation and membrane rupture compared to the untreated strains.

Additionally, the bacteria membrane surface potential became neutralized and this led to higher surface tension, abnormal structure, rapturing and damage on bacterial cells membrane.

3.4. Nanoparticles induces production of reactive oxygen species

The AO/EtBr staining technique was used to detect generation of ROS after the bacterial strains were treated with Au NPs, ZnO NPs, Cur NPs, Au/ZnO NPs, and Cur-Au/ZnO CSNPs. The indicators that show the presence of ROS are nitric oxide and hydrogen peroxide. When AO/EtBr dye comes into contact with reactive oxygen species, produced when an organism is under stress, it undergoes oxidation. The EtBr component will only pervade cells whose membrane integrity has been damaged and reacts with cells nucleic acid. The dead cells are stained in red while the viable cells are stained green. The bacterial strains that treated with Au NPs, ZnO NPs, Cur NPs, Au/ZnO NPs, and Cur-Au/ZnO CSNPs showed generation in ROS compared to the untreated cells. The Au NPs, ZnO NPs, Cur NPs, Au/ZnO NPs, and Cur-Au/ZnO CSNPs treated *S.aureus* resulted in more structural deformities as well as higher levels of ROS production as in Fig. 8, as demonstrated by a high number of bacteria strains that are reddish. Overall, the results showed that Au NPs, ZnO NPs, Cur NPs, Au/ZnO NPs, and Cur-Au/ZnO CSNPs were suitable as antibacterial agents that can be applied in biomedical and biological fields.

3.5. Nanoparticles attenuated invasion of bacterial strain to REF cells

REF cells were pretreated with Au, ZnO, Cur, Au/ZnO NPs and Cur-Au/ZnO CSNPs for 1 h and then infected with bacterial strains at MOI (200:1) for 1 h. The results shows that the Au, ZnO, Cur, Au/ZnO NPs and Cur-Au/ZnO CSNPs are attenuated the binding of bacterial strains to REF cells as indicated in Fig. 9. To determine whether Au, ZnO, Cur, Au/ZnO NPs and Cur-Au/ZnO also inhibit the invasion of bacterial strains, REF cells were pretreated with Au, ZnO, Cur, Au/ZnO NPs and Cur-Au/ZnO for 1 h and then infected with bacterial strains for 3 h. The cell invasion of bacterial strains in the presence and absence of Au, ZnO, Cur, Au/ZnO NPs and Cur-Au/ZnO CSNPs was significantly decreased as shown in Fig. 10. Taken together, these results of present study demonstrated that the Au, ZnO, Cur, Au/ZnO NPs and Cur-Au/ZnO mediate the adherence and invasion of bacterial strain in REF cells.

3.6. Nanoparticles blocks *S. aureus* α-Hemolysin production

As shown in Fig. 11, treatment with Au NPs, ZnO NPs, Cur NPs, Au/ZnO NPs, and Cur-Au/ZnO CSNPs attenuated the α-Hemolysin activity. Western blot analysis was performed to verify whether the decreased hemolytic activities of *S. aureus*. The results showed the ability of prepared Au NPs, ZnO NPs, Cur NPs, Au/ZnO NPs, and Cur-Au/ZnO CSNPs in reduction of production of α-Hemolysin.

3.7. Nanoparticles prevents S. aureus mediated alveolar epithelial cell injury

The ability of prepared Au NPs, ZnO NPs, Cur NPs, Au/ZnO NPs, and Cur-Au/ZnO CSNPs to prevent α-Hemolysin-mediated alveolar epithelial cell injury was tested using co-culture system. As in Fig. 12, upon co-culturing with *S. aureus*, cell death was evident, as indicated by an increase in the number of orange-red fluorescent dead cells and a transform in the cellular morphology of the live cells. Remarkably, after added of Au NPs, ZnO NPs, Cur NPs, Au/ZnO NPs, and Cur-Au/ZnO CSNPs in the co-culture system conferred a robust protection against *S. aureus*-mediated cell injury. Furthermore, to measure the ability of Au NPs, ZnO NPs, Cur NPs, Au/ZnO NPs, and Cur-Au/ZnO CSNPs to inhibits the effect of *S. aureus* on A549 cells. LDH release from A459 was tested using a LDH release assay, and the results are showed as percentage of cell death Fig. 13. The results showed the ability of Au NPs, ZnO NPs, Cur NPs, Au/ZnO NPs, and Cur-Au/ZnO CSNPs to reduce the percentage of LDH release when added to the co cultures of A549 cells and *S. aureus*.

3.8. Cur-Au/ZnO CSNPs improves lung injury in *S. aureus*

In the present study, we investigated the in vivo effects on *S. aureus* in a mouse model, the lung tissue of mice that infected with *S.aureus* then received PBS was kermesinus and had a firm texture as in shown in Fig. 14-B, the mice that were treated with PBS typically revealed that significant alveolar destruction had occurred along with infiltration of large numbers of inflammatory cells. Notably, the alveoli were open and contained no large areas of inflammation, although occasionally small areas of congestion were observed in Au NPs, ZnO NPs, Cur NPs, Au/ZnO NPs, and Cur-Au/ZnO CSNPs -treated mice as shown in Fig. 14 (C, D, E, F, and G).

4. Conclusion

In conclusion, Gold with Zinc Oxide nanoparticles (Au@ZnO NPs) were prepared by laser ablation then capped with Curcumin nanoparticles. This study investigated the antibacterial activity of Nano-curcumin-Au/ZnO nanocomposite against *S.aureus*. The bacterial cytoplasmic membrane and nucleic acid were penetrated by tested nanoparticles, resulting in bacterial strain destruction. Additionally, in the current study we investigated the activity of Cur-Au@ZnO NPs against bacterial α-Hemolysin toxin. The results demonstrated that the Cur-Au@ZnO NPs is a potent inhibitor of α-hemolysin secreted by *S. aureus*. So, Cur-Au@ZnO NPs mediated inhibition of α-Hemolysin production may offer a new strategy in combating pathogen infections. The Cur-Au@ZnO could serve as a potential antibacterial agent in future for biomedical applications.

References

1. S.L. Logunov, T.S. Ahmadi, M.A. El-Sayed, J.T. Khoury, R.L. Whetten, J. Phys. Chem. B **101**, 3713–3719 (1997)
2. C. Burda, X. Chen, R. Narayanan, M.A. El-Sayed, Chem. Rev. **105**, 1025–1102 (2005)
3. T.M. Rashid, U.M. Nayef, M.S. Jabir, F.A. Mutlak, March. *Journal of Physics: Conference Series*. Vol. 1795, No. 1, p. 012041, (2021)

4. P. Wagener et al., J. Phys. Chem. C **114.17**, 7618–7625 (2010)
5. A.A. Menazea, I.S. Elashmawi, F. H. Abd El-kader, and N. A. Hakeem. J. Inorg. Organomet. Polym Mater. **28**(6), 2564–2571 (2018)
6. M.M. ElFaham, M. Okil, M. Ayman, Mostafa, Opt. Laser Technol. **108**, 634–641 (2018)
7. L. Song et al., Talanta **146**, 285–290 (2016)
8. R. Varghese et al., Saudi journal of biological sciences **26**(1), 148–154 (2019)
9. T.V. Verissimo, N.T. Santos, J.R. Silva, R.B. Azevedo, A.J. Gomes, C.N. Lunardi, Mater. Sci. Eng. C **65**, 199–204 (2016)
10. I. Fratoddi et al., Nano Research **8.6**, 1771–1799 (2015)
11. J.F. Hainfeld et al., Br. J. Radiol. **79**, 939: 248–253 (2006)
12. A. Kumar, X. Zhang, X.J. Liang, Biotechnol, Adv. **31**, 593–606 (2013)
13. I. Khalil, N.M. Julkapli, W.A. Yehye, W.J. Basirun, S.K. Bhargava, Materials **9**, 406 (2016)
14. T.G. Smijs, S. Pavel, Nanotechnology, Science and Applications **4**, 95–112 (2011)
15. A. Hatamie, A. Khan, M. Golabi et al., Langmuir, vol. 31, no. 39, pp. 10913–10921, (2015)
16. S.K. Sethi, G. Manik, *Polymer-Plastics Technology and Engineering*, *57*(18), pp.1932–1952, (2018)
17. H.K. Syed, K.B. Liew, G.O.K. Loh, K.K. Peh, Food Chem. **170**, 321–326 (2015)
18. T. Wei, Khang, S. Manickam, Asia-Pacific journal of chemical engineering **7**, S125–S133 (2012)
19. C. Mangolim, Sampaio et al., Food Chem. **153**, 361–370 (2014)
20. E. Rubinstein, Marin H. Kollef, and Dilip Nathwani. *Clinical Infectious Diseases* 46. Supplement_5: S378-S385, (2008)
21. M.H. Kollef et al., Chest **128.6**, 3854–3862 (2005)
22. F.A. Orrett, M. Land, BMC Infect. Dis. **6**(1), 1–6 (2006)
23. R.J. Gordon, F.D. Lowy. *Clinical infectious diseases* 46.Supplement_5:S350-S359, (2008)
24. A. Hildebrand, M. Pohl, S. Bhakdi, J. Biol. Chem. **266**, 26: 17195–17200 (1991)
25. E. Gouaux, J. Struct. Biol. **121**, 2: 110–122 (1998)
26. M.C. McElroy et al., Infect. Immun. **67**, 10: 5541–5544 (1999)
27. J. Wardenburg, R.J. Bubeck, Patel, O. Schneewind, Infect. Immun. **75**(2), 1040–1044 (2007)
28. C.C. McCormick et al., Investig. Ophthalmol. Vis. Sci. **50**, 6: 2848–2854 (2009)
29. S.B. Park et al., Journal of nanobiotechnology **16**(1), 1–14 (2018)
30. E. Yazar et al., *VETERINARNI MEDICINA-PRAHA*- 51.2: 51, (2006)
31. D. Hu et al., ACS Nano **11.9**, 9330–9339 (2017)
32. M.M. Alves et al., ACS Appl. Mater. Interfaces **9**, 34: 28157–28167 (2017)
33. V. Aurore et al., Nanomed. Nanotechnol. Biol. Med. **14.2**, 601–607 (2018)
34. R. Baskaran, T. Madheswaran, P. Sundaramoorthy, Hwan Mook Kim, and Bong Kyu Yoo. Int. J. Nanomed. **9**, 3119 (2014)

35. G.M. Sulaiman, S. Majid, Jabir, H. Anaheed Hameed. *Artificial cells, nanomedicine, and biotechnology* 46, no. sup1: 708–720, (2018)
36. W.K. Kadhim, U.M. Abdul, Nayef, M.S. Jabir, Surf. Rev. Lett. **26**(10), 1950079 (2019)
37. M.A. Gondal, Q.A. Drmosh, Z.H. Yamani, T.A. Saleh, Applied surface science **256**(1), 298–304 (2009)
38. Q.A. Drmosh, M.A. Gondal, Z.H. Yamani, T.A. Saleh, Appl. Surf. Sci. **256**, no. 14: 4661–4666 (2010)
39. H. Kumar, R. Rani, International Letters of Chemistry, Physics and Astronomy **14**, 26–36 (2013)
40. W.P.T.D. Perera, K. Ranga, U.I. Dissanayake, N.M. Ranatunga, K.D.C. Hettiarachchi, J.M. Perera, R.T. Unagolla, De Silva, L.R. Pahalagedara, RSC Advances **10**, no. 51: 30785–30795 (2020)
41. E. Solati, L. Dejam, D. Dorranian, Opt. Laser Technol. **58**, 26–32 (2014)
42. P. Singh, K. Kumar, Wani, Ruchika Kaul-Ghanekar, Asmita Prabhune, and Satishchandra Ogale. RSC Advances **4**, no. 104: 60334–60341 (2014)
43. H.H. Bahjat, R.A. Ismail, G.M. Sulaiman, M. Jabir S. 1–8 (2021). Journal of Inorganic and Organometallic Polymers and Materials
44. K.S. Khashan, G.M. Sulaiman, S.A. Hussain, T.R. Marzoog, M.S. Jabir, *30*(9), 3677–3693, (2020). Journal of Inorganic and Organometallic Polymers and Materials
45. A. Younus, S. Al-Ahmer, M. Jabir, *14*, 131–133.(2019). Research Journal of Biotechnology
46. M.S. Jabir, U.M. Nayef, K.H. Jawad, Z.J. Taqi, N.R. Ahmed, 454, No. 1, p. 012077, (2018). In IOP Conference Series: Materials Science and Engineering
47. M.S. Jabir, U.M. Nayef, W.K. Abdulkadhim, Z.J. Taqi, G.M. Sulaiman, U.I. Sahib, C.C. Su, 1–19 (2020). Journal of Inorganic and Organometallic Polymers and Materials
48. I.H. Ali, M.S. Jabir, H. Al-Shmgani, G.M. Sulaiman, A.H. Sadoon 1003012009. (2018). *Journal of Physics: Conference Series*
49. S.H. Kareem, A.M. Naji, Z.J. Taqi, M.S. Jabir, *30*(12), 5009–5023, (2020). Journal of Inorganic and Organometallic Polymers and Materials
50. M.A. Gondal, Q.A. Drmosh, Z.H. Yamani, T.A. Saleh, Applied surface science **256**(1), 298–304 (2009)
51. Q.A. Drmosh, M.A. Gondal, Z.H. Yamani, T.A. Saleh, Appl. Surf. Sci. **256**, no. 14: 4661–4666 (2010)
52. H. Kumar, R. Rani, International Letters of Chemistry, Physics and Astronomy **14**, 26–36 (2013)
53. W.P.T.D. Perera, K. Ranga, U.I. Dissanayake, N.M. Ranatunga, K.D.C. Hettiarachchi, J.M. Perera, R.T. Unagolla, De Silva, L.R. Pahalagedara, RSC Advances **10**, no. 51: 30785–30795 (2020)
54. E. Solati, L. Dejam, D. Dorranian, Opt. Laser Technol. **58**, 26–32 (2014)
55. P. Singh, K. Kumar, Wani, Ruchika Kaul-Ghanekar, Asmita Prabhune, and Satishchandra Ogale. RSC Advances **4**, no. 104: 60334–60341 (2014)

Figures

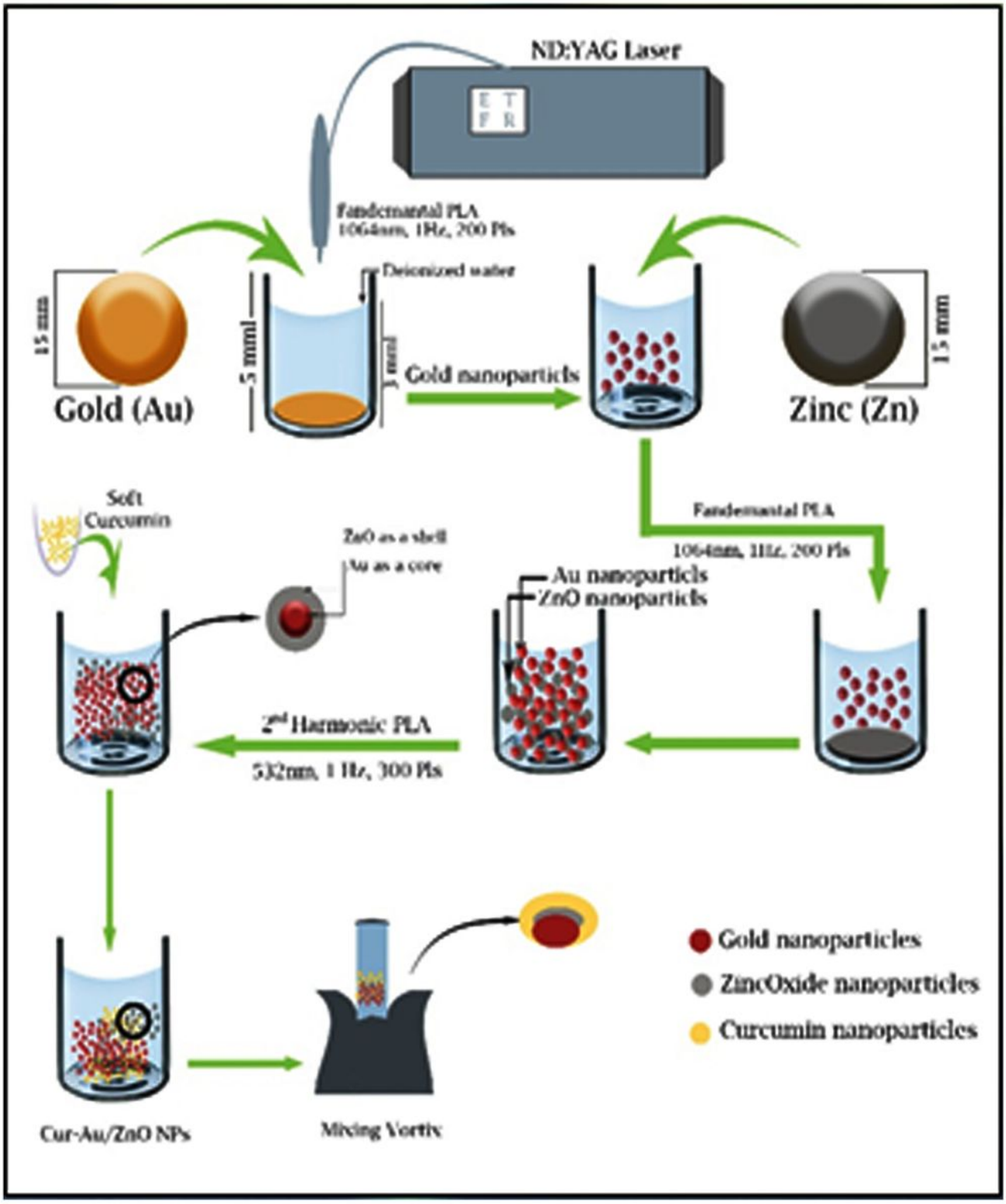

Figure 1

Steps of prepared Cur-Au/ZnO NPs.

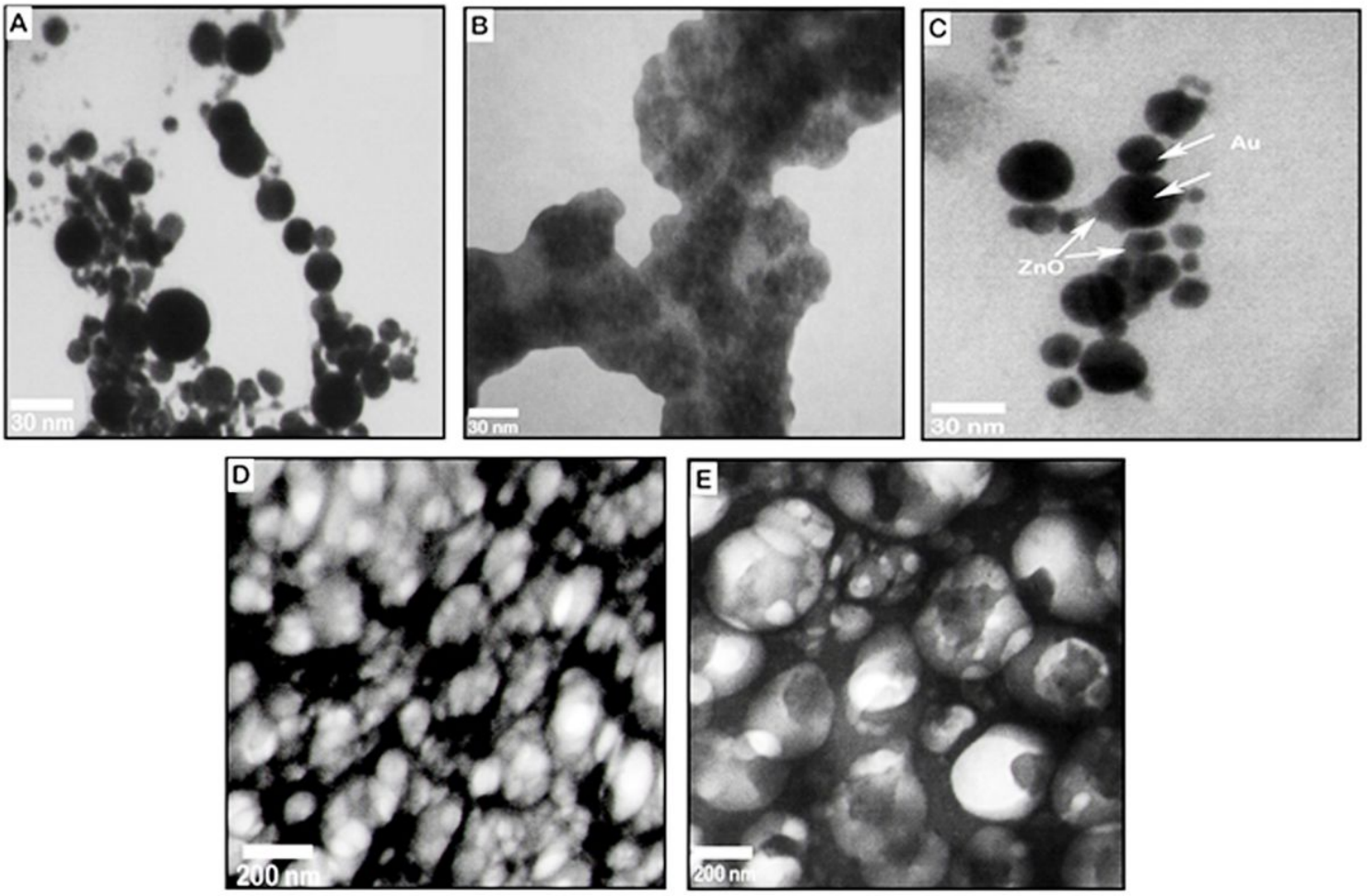

Figure 2

TEM images of A- Au NPs, B- ZnO NPs, C- Au/ZnO NPs, D-Cur-NPs, E, Cur-Au/ZnO NPs.

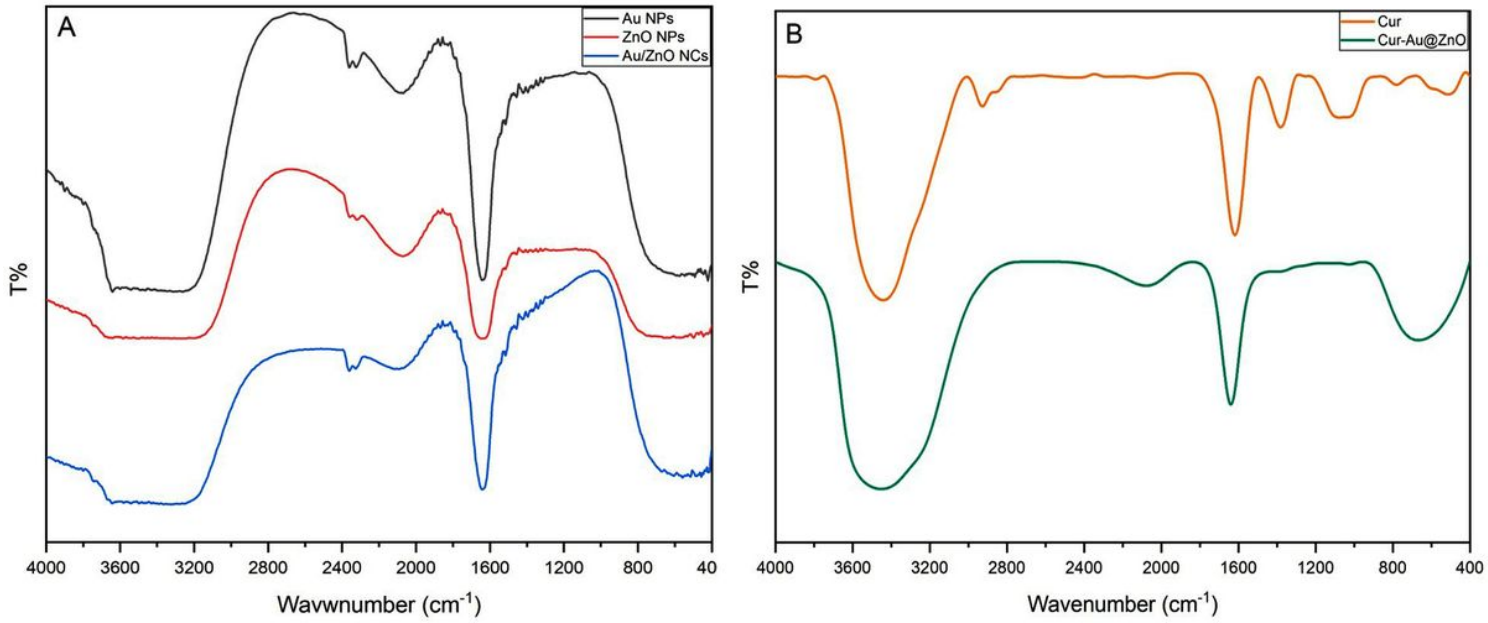

Figure 3

FTIR spectrum of Au NPs, ZnO NPs, Au/ZnO NPs, Cur-NPs, Cur-Au/ZnO NPs.

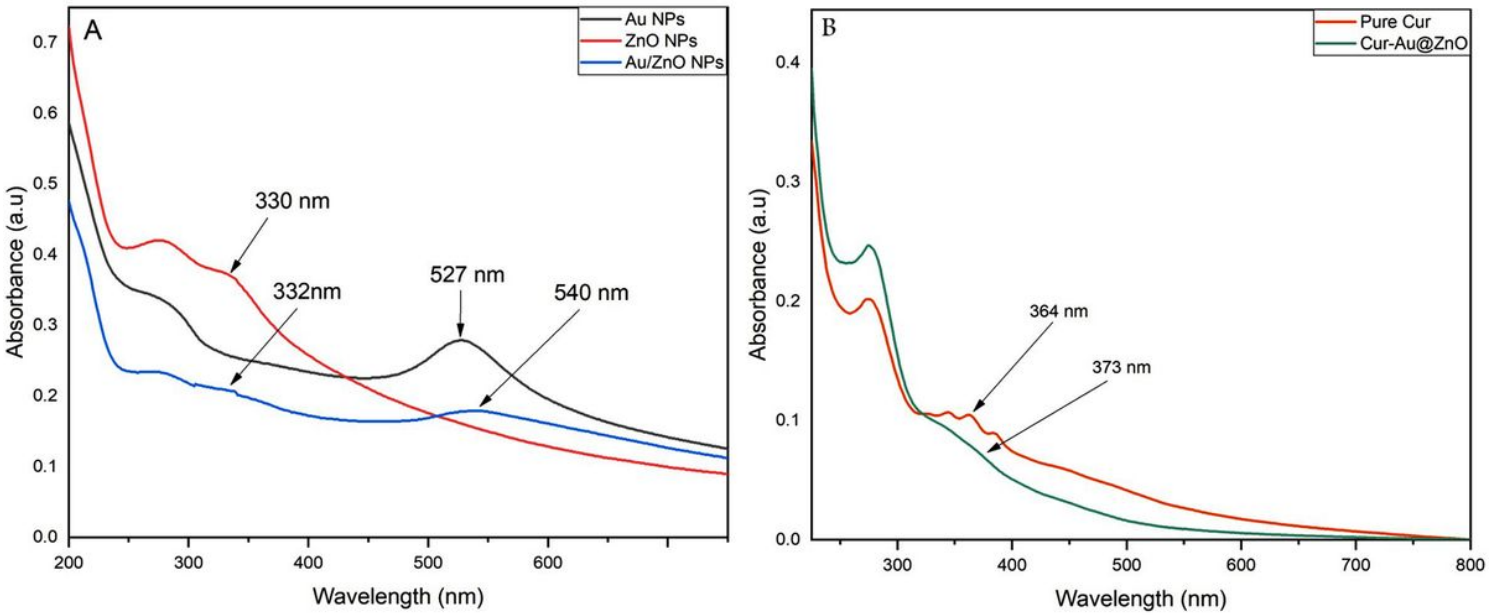

Figure 4

UV-Vis absorption spectrum of Au NPs, ZnO NPs, Au/ZnO NPs, Cur-NPs, Cur-Au/ZnO NPs.

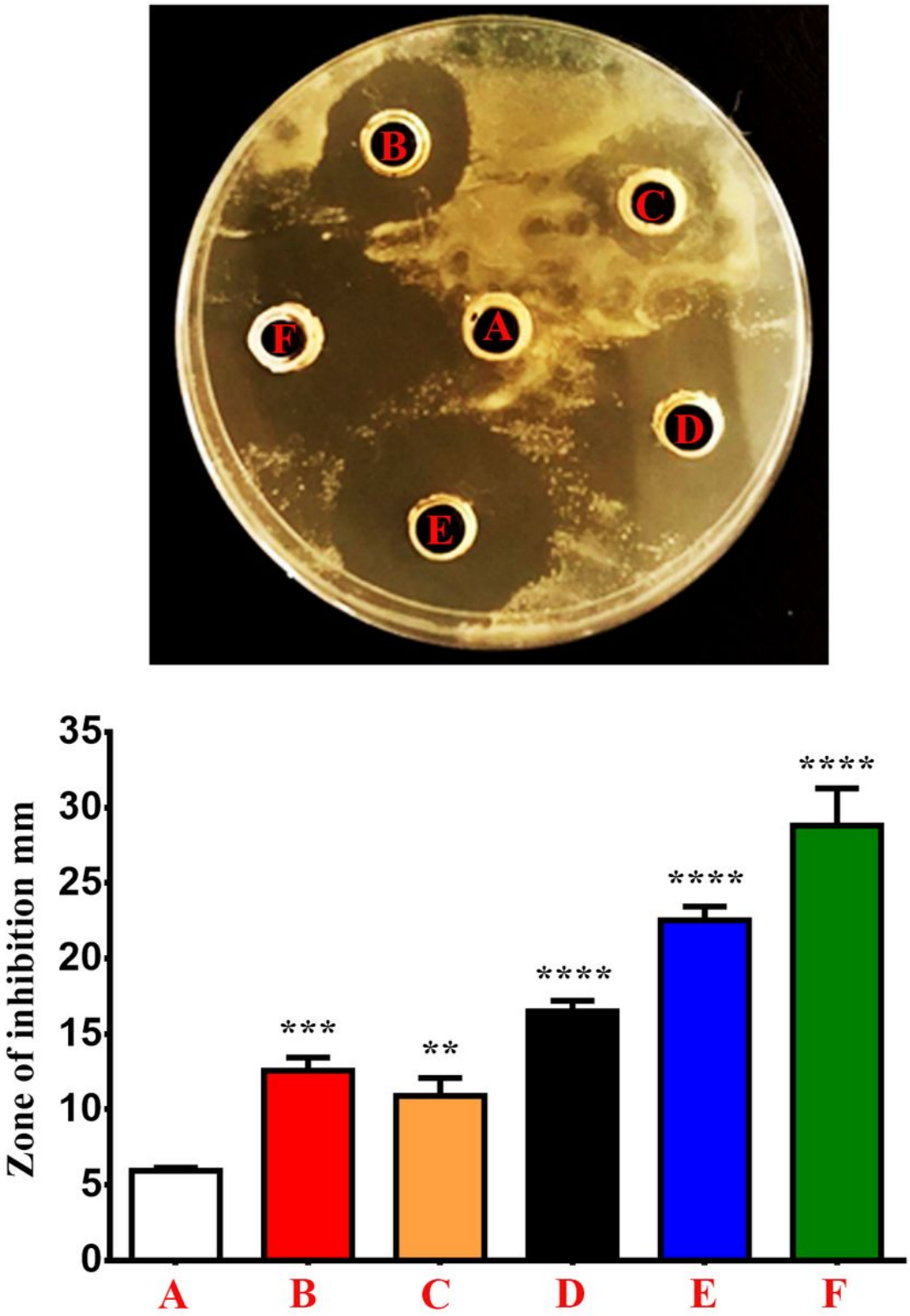

Figure 5

Anti-bacterial activity of prepared NPs against S.aureus. A,control untreated bacterial strain. B, Bcterial strain treated with ZnO NPs, C, bacterial strains with Cur-NPs, D, bacterial strains treated with Au NPs. E, bacterial strains treated with Au/ZnO NPs. F, bacterial strains treated with Cur-Au/ZnO NPs . The data are shown as the mean±SD. **p<0.01, ***p<0.001, and ****p<0.0001.

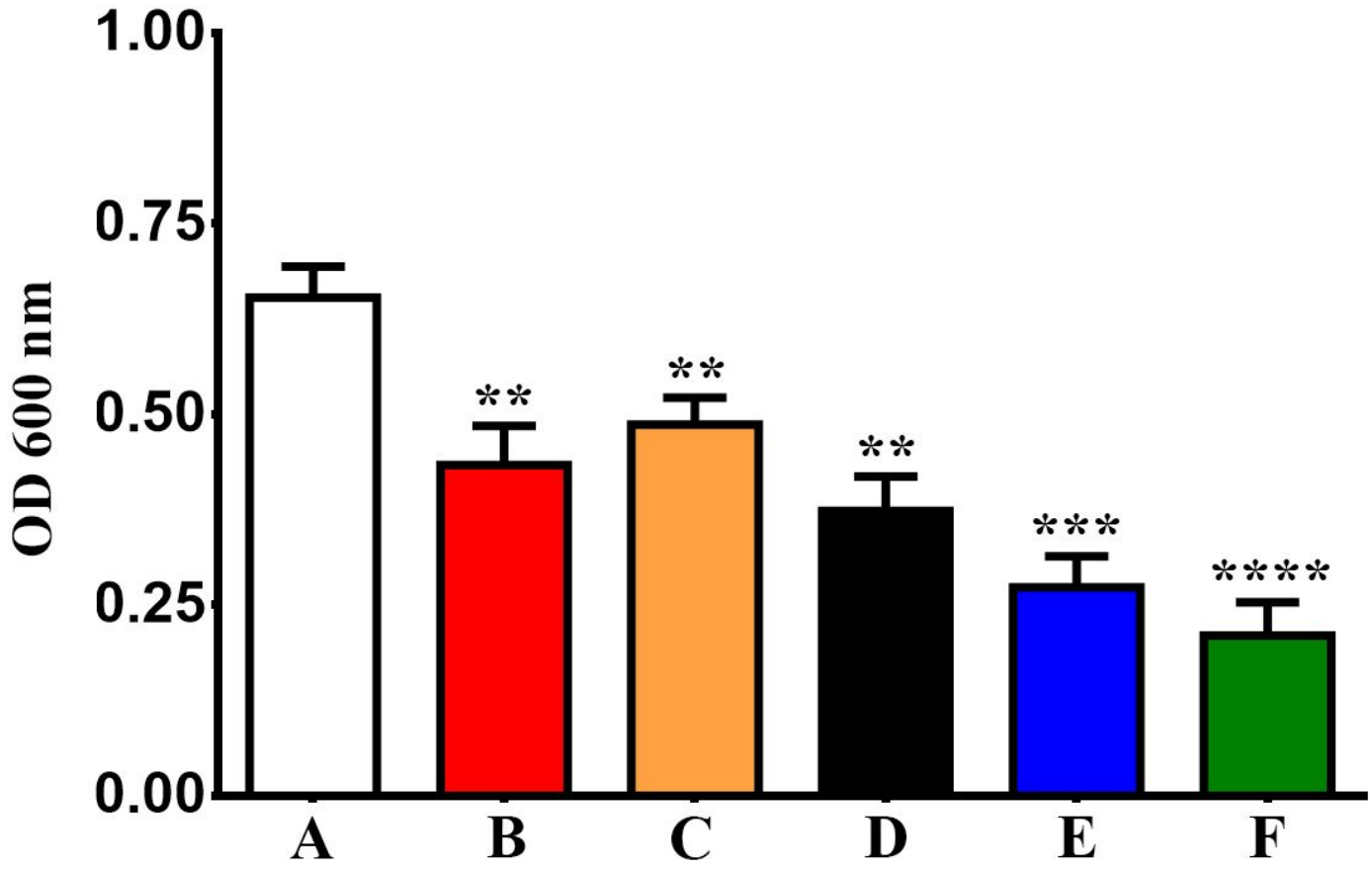

Figure 6

Effect of prepared NPs in growth rate of S.aureus. A,control untreated bacterial strain. B, Bcterial strain treated with ZnO NPs, C, bacterial strains with Cur-NPs, D, bacterial strains treated with Au NPs. E, bacterial strains treated with Au/ZnO NPs. F, bacterial strains treated with Cur-Au/ZnO NPs.

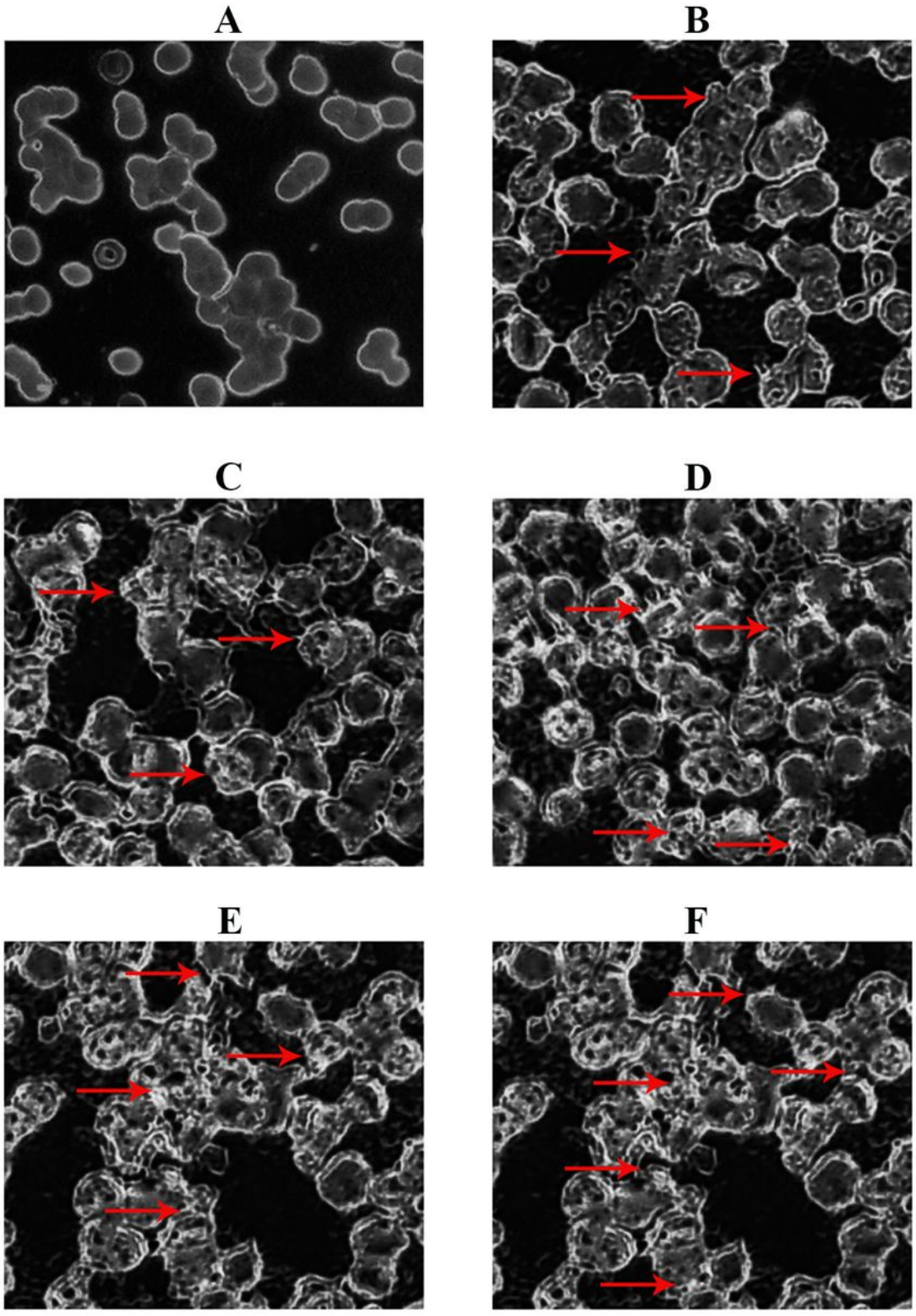

Figure 7

SEM images visualized of NPs treated S.aureus. Treated bacterial strain showing membrane damage. Membrane blabbing's and membrane clumping. A,control untreated bacterial strain. B, Bcterial strain treated with ZnO NPs, C, bacterial strains with Cur-NPs, D, bacterial strains treated with Au NPs. E, bacterial strains treated with Au/ZnO NPs. F, bacterial strains treated with Cur-Au/ZnO NPs.

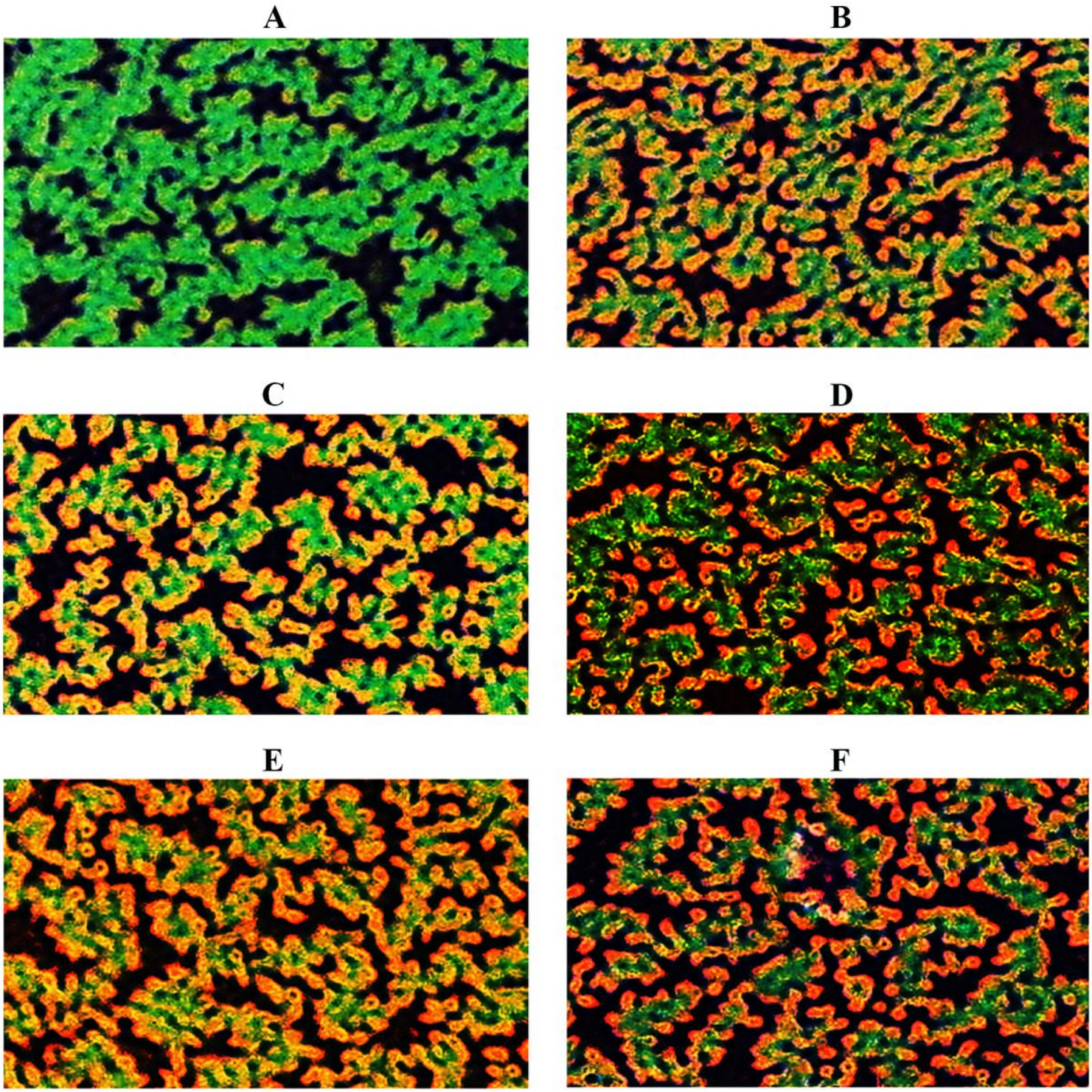

Figure 8

Fluorescence microscopic images of the green and red fluorescence stained S.aureus. A,control untreated bacterial strain. B, Bcterial strain treated with ZnO NPs, C, bacterial strains with Cur-NPs, D, bacterial strains treated with Au NPs. E, bacterial strains treated with Au/ZnO NPs. F, bacterial strains treated with Cur-Au/ZnO NPs. Magnification power 40x.

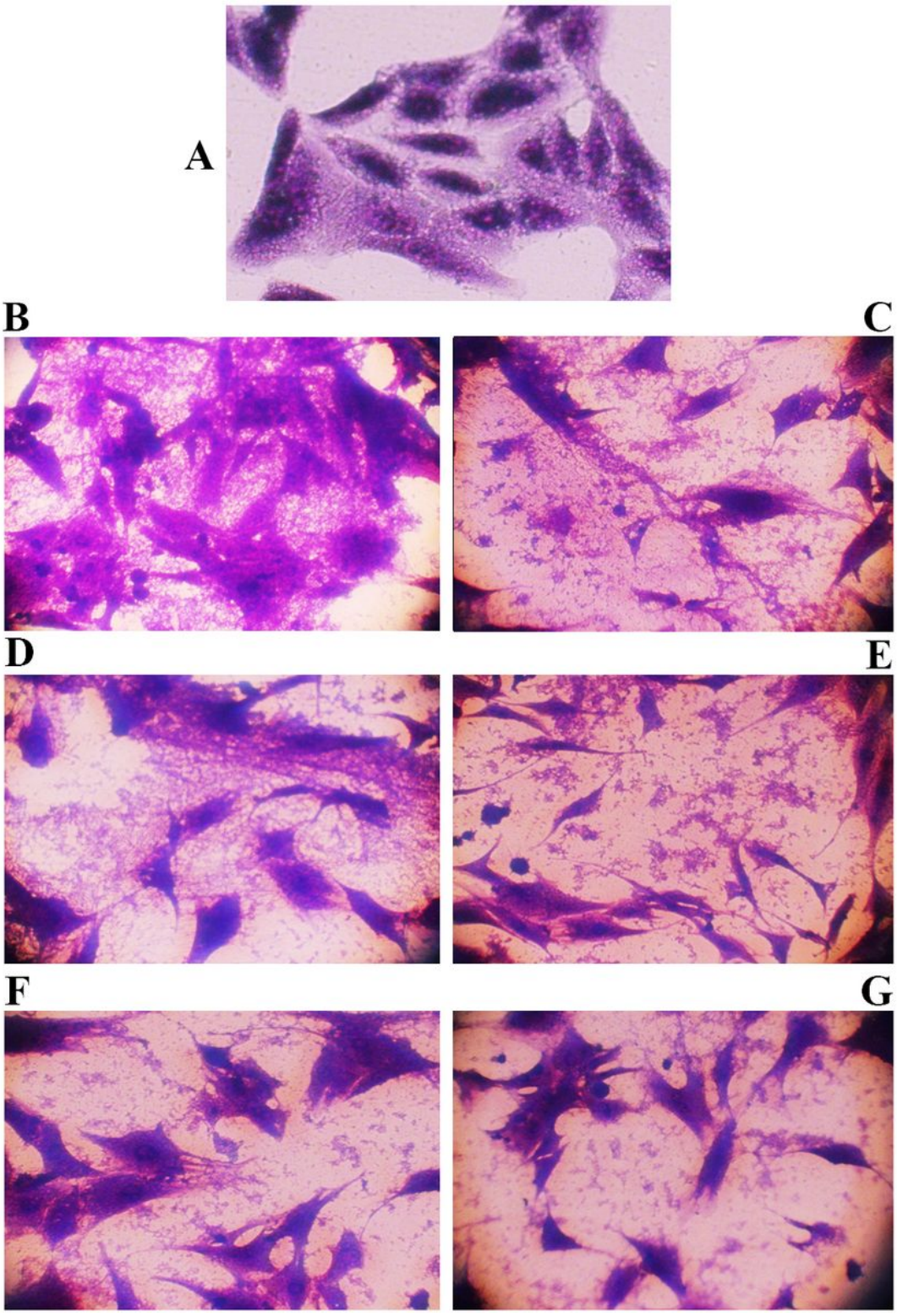

Figure 9

Nanoparticles inhibits invasion of bacterial strains in REF cells as indicated. A, Control REF cells, B, REF infected with S.aureus. C, REF cells pre- treated with ZnO NPs then infected with bacterial strains. D, REF cells pre- treated with Cur-NPs then infected with bacterial strains. E, REF cells pre- treated with AuNPs then infected with bacterial strains. F, REF cells pre- treated with Au/ZnO NPs then infected with bacterial

strains. G, REF cells pre- treated with Cur-Au/ZnO NPs then infected with bacterial strains. Magnification power 40x.

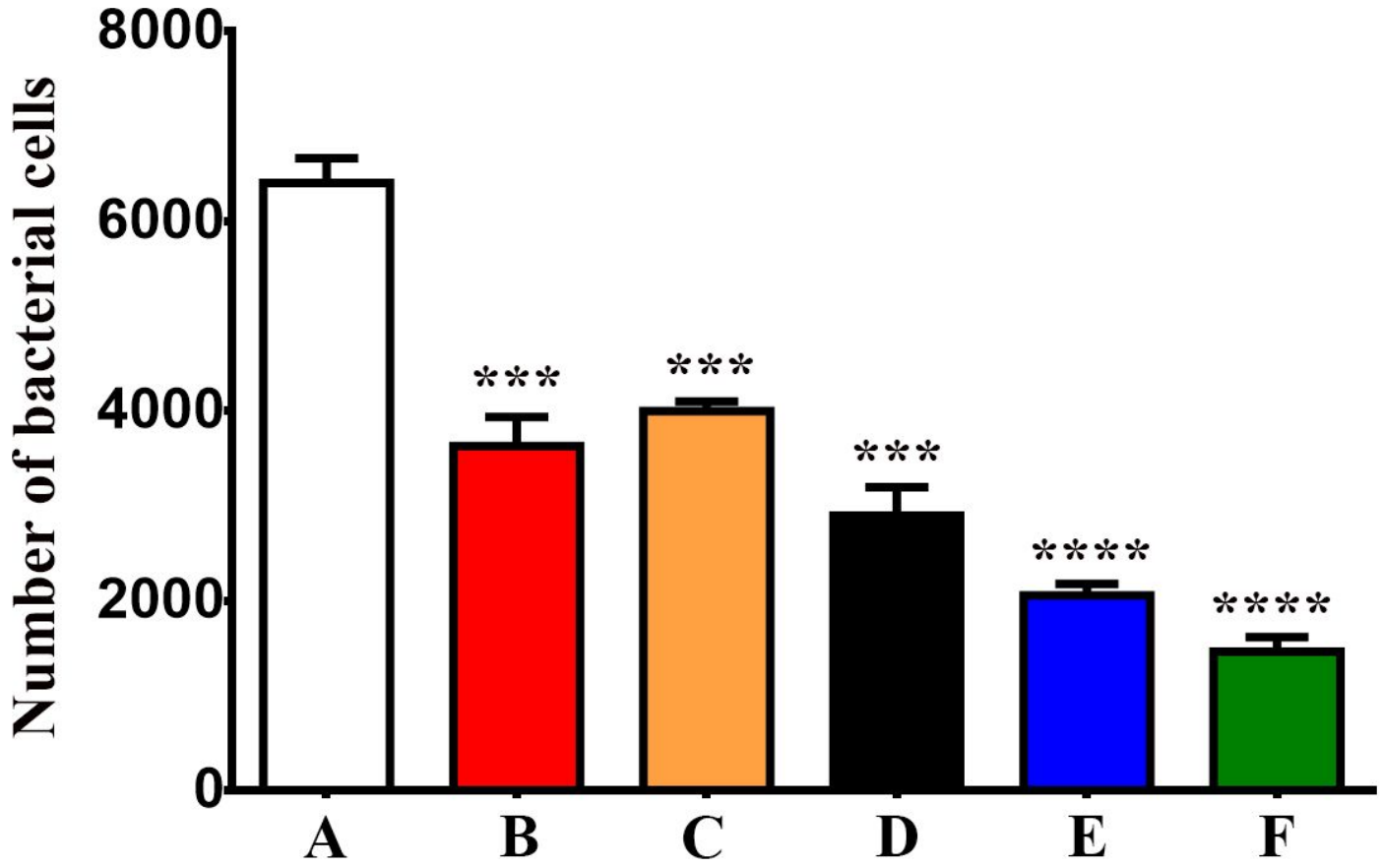

Figure 10

Prepared nanoparticles decreases interaction of S. aureus with REF cells as indicated. A, Control REF cells, B, REF infected with S.aureus. C, REF cells pre- treated with ZnO NPs then infected with bacterial strains. D, REF cells pre- treated with Cur-NPs then infected with bacterial strains. E, REF cells pre- treated with AuNPs then infected with bacterial strains. F, REF cells pre- treated with Au/ZnO NPs then infected with bacterial strains. G, REF cells pre- treated with Cur-Au/ZnO NPs then infected with bacterial strains. The value are shown as the mean±SEM. ***p<0.001, ****p<0.0001.

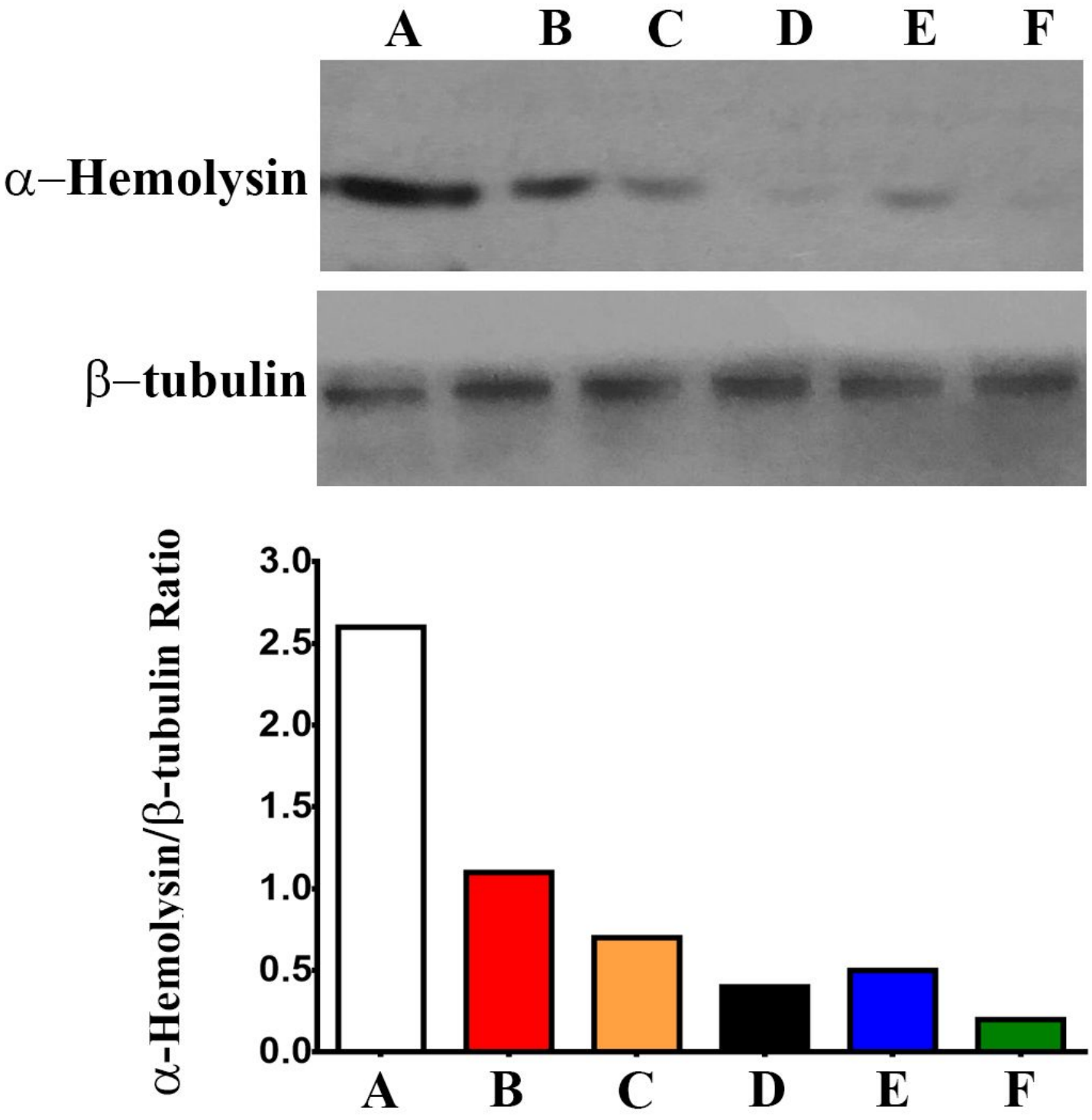

Figure 11

Prepared nanoparticles reduces production of α-Hemolysin. Western blot analysis of α-Hemolysin. A, control bacterial strain. B, Bcterial strain treated with ZnO NPs, C, bacterial strains with Cur-NPs, D, bacterial strains treated with Au NPs. E, bacterial strains treated with Au/ZnO NPs. F, bacterial strains treated with Cur-Au/ZnO NPs. Graph represented densitometry quantification of the α-Hemolysin /b-tubulin ratio, as indicated.

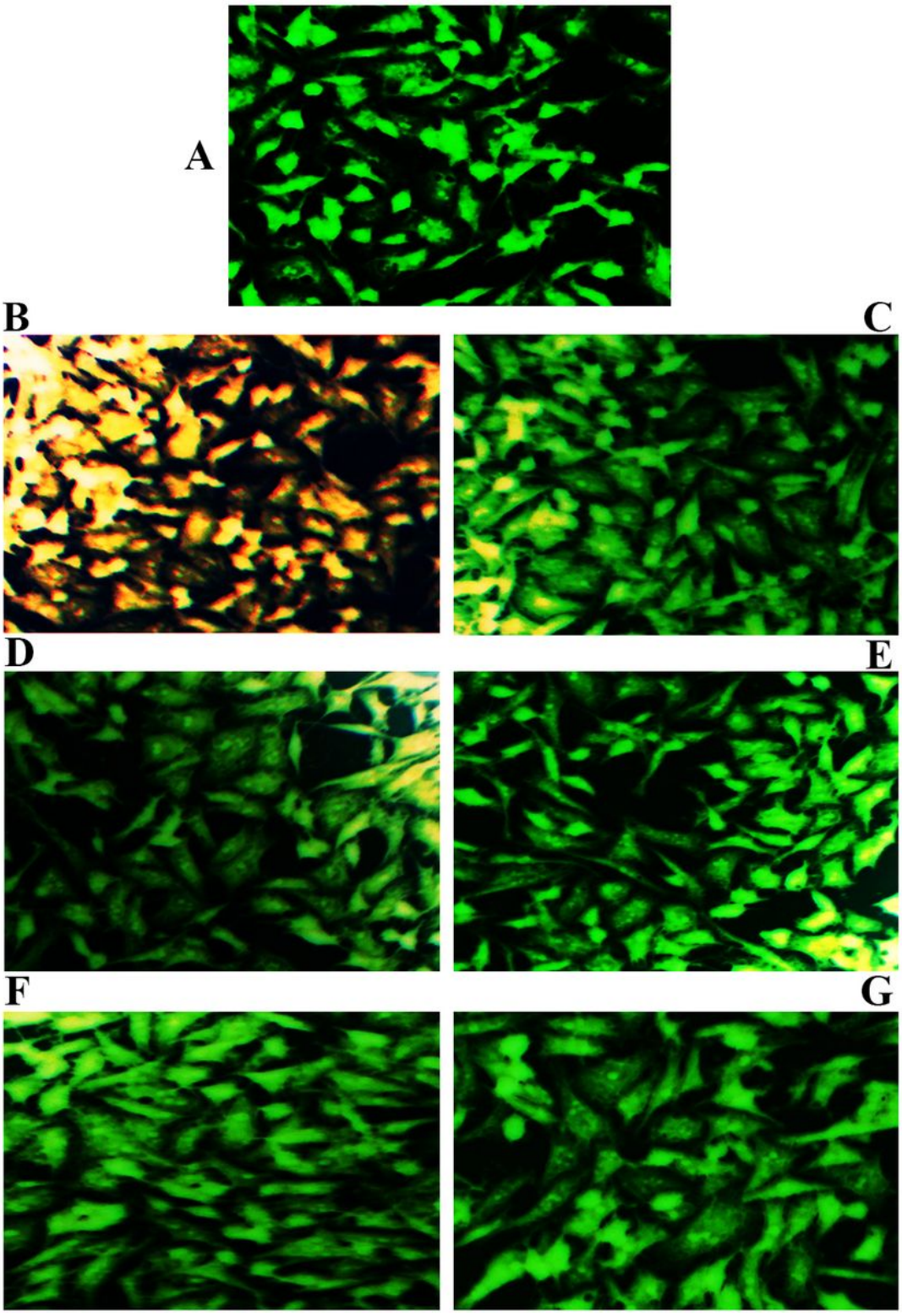

Figure 12

Cur-Au/ZnO NPs blocked S. aureus mediated lung cell injury. A, Control A549 cells, B, A549 cells infected with S.aureus. C, A549 cells pre- treated with ZnO NPs then infected with S.aureus. D, A549 cells pre-treated with Cur-NPs then infected with S.aureus. E, A549 cells pre- treated with AuNPs then infected with S.aureus. F, A549 cells pre- treated with Au/ZnO NPs then infected with S.aureus. G, A549 cells pre-treated with Cur-Au/ZnO NPs then infected with S.aureus. Scale bare 50 μm.

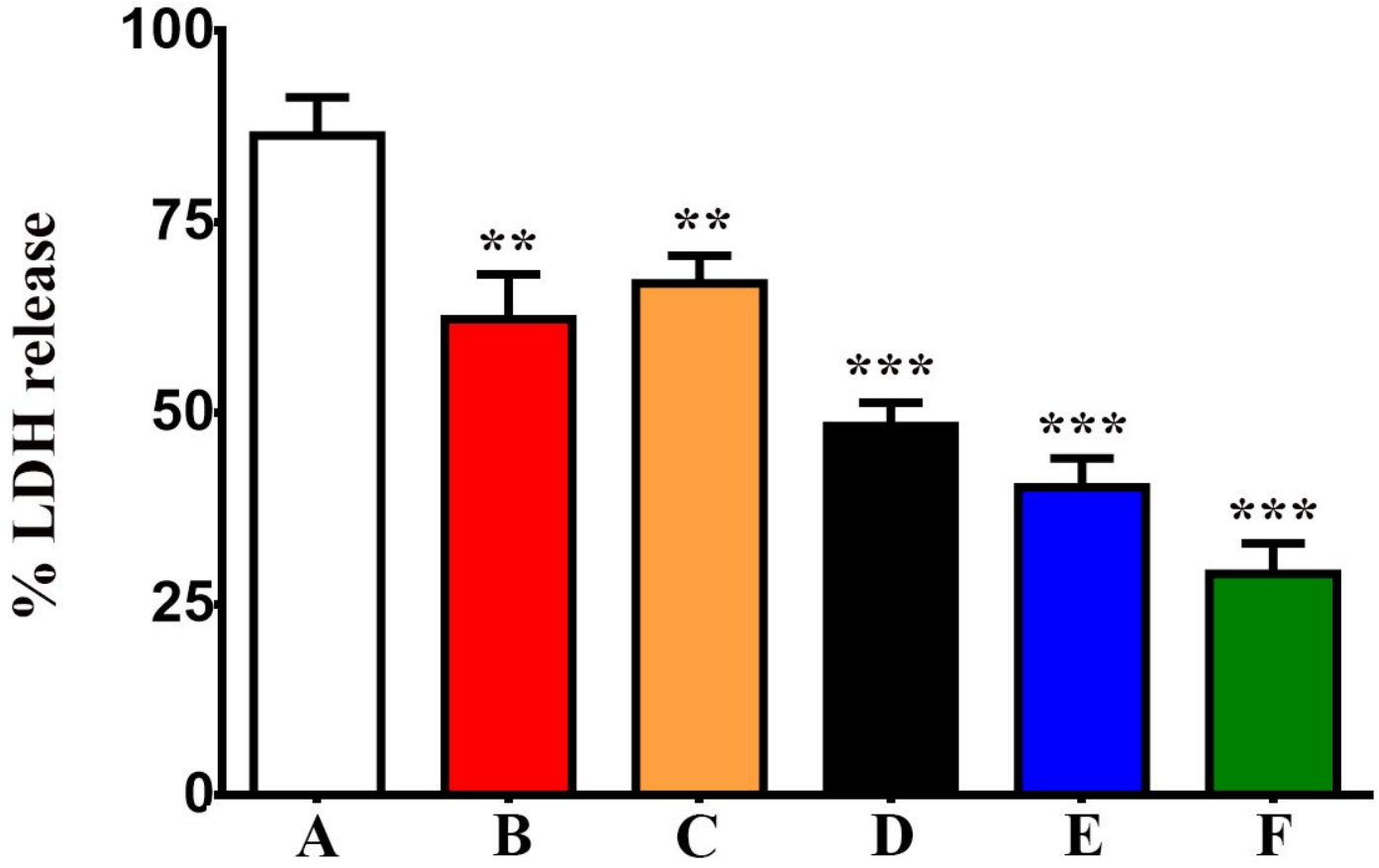

Figure 13

Cur-Au/ZnO NPs reduces LDH release in A549 cells. A, A549 cells infected with S.aureus. B, A549 cells pre- treated with ZnO NPs then infected with S.aureus. C, A549 cells pre- treated with Cur-NPs then infected with S.aureus. D, A549 cells pre- treated with AuNPs then infected with S.aureus. E, A549 cells pre- treated with Au/ZnO NPs then infected with S.aureus. F, A549 cells pre- treated with Cur-Au/ZnO NPs then infected with S.aureus. The data are shown as the mean±SD. **p<0.01, ***p<0.001.

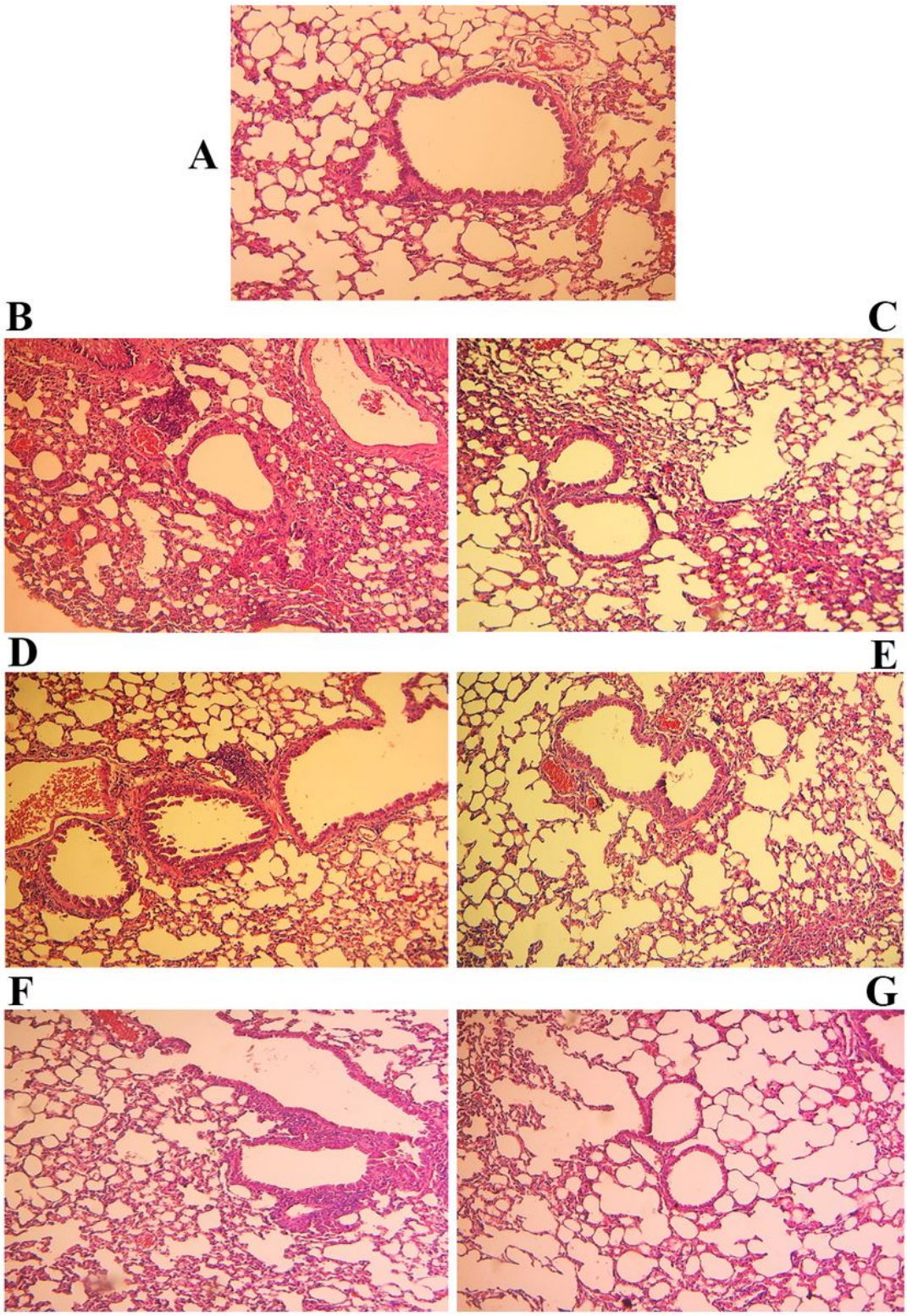

Figure 14

Cur-Au/ZnO NPs improves lung injury. Histopathological changes in lung sections.A, Control mice lung, B, Mice were infected with S.aureus via intranasal route. C, Mice were infected with S.aureus via intranasal route then treated with ZnO NPs. D, Mice were infected with S.aureus via intranasal route thene treated with Cur-NPs. E, Mice were infected with S.aureus via intranasal route then treated with AuNPs. F, Mice were infected with S.aureus via intranasal route then treated with Au/ZnO NPs. G, Mice were infected with

S.aureus via intranasal route then treated with Cur-Au/ZnO NPs. Section were stained by H and E stain. Magnification power 10x.